Pergamon

Int. J. Solids Structures Vol. 34, No. 17, pp. 2131–2160, 1997

Printed in Great Britain
0020–7683/97 $17.00 + .00

PII: S0020–7683(96)00118–7

ENDOCHRONIC DESCRIPTION FOR VISCOPLASTIC BEHAVIOR OF MATERIALS UNDER MULTIAXIAL LOADING

W. F. PAN and C. H. CHERN
Department of Engineering Science, National Cheng Kung University, Tainan, Taiwan, 70101, Republic of China

(*Received* 6 *October* 1995; *in revised form* 10 *June* 1996)

Abstract—A new formulation of the rate-sensitivity function of the intrinsic time measure is presented in this paper. The endochronic theory is extended to simulate the viscoplastic behavior of material under multiaxial loading. The rate-sensitivity function proposed by Wu and Yip [Wu, H. C. and Yip, M. C. (1980). Strain-rate and strain-rate history effects on the dynamic behavior of metallic materials. *Int. J. Solids Struct.* **16,** 515–536] is shown to be identical to the new formulation of the rate-sensitivity function under uniaxial loading. The first-order ordinary differential constitutive equations of endochronic theory, as derived by Valanis [Valanis, K. C. (1979). Endochronic theory with proper loop closure properties. *System Science and Software Report SSS-R*-80-4182 (1984). Continuum foundations of plasticity. *ASME J. Engng Mater. Technol.* **106,** 367–375], are used in this study. Constitutive equations for combined axial-torsional and biaxial strain-paths are derived. Experimental data found in literature of OHFC copper for rate-independent behavior and 304 stainless steel for viscoplastic response are used for comparison. It is shown that most of the viscoplastic behaviors of materials can be adequately described by the theory. © 1997 Elsevier Science Ltd.

1. INTRODUCTION

The endochronic theory was first proposed by Valanis (1971) for describing the material behavior under elastic–plastic deformation. The theory is based on the irreversible thermodynamics of internal variables and the concept of intrinsic time. The intrinsic time, as originally defined by total strain tensor, has led to a discrepancy with the experimental data in the case of unloading. Valanis (1980) reformulated the definition of intrinsic time by plastic strain tensor, the theory has been extended widely to simulate various material responses. The composition of a delta function and decaying exponential functions of the kernel function were also introduced, the correlation with the classical theory of plasticity was subsequently achieved. Various versions of the classical theory of plasticity with isotropic or kinematic hardening rules or their combinations are shown to be particular cases of the theory.

Thereafter, many investigations involving various materials subjected to diverse loading histories were undertaken for evaluating the theoretical application. The stress–strain behaviors for metals [Wu and Yip (1981); Wu and Yang (1983); Valanis and Lee (1984); Wu *et al.* (1985); Fan and Peng (1991)], concretes [Bazant and Bhat (1976); Valanis and Read (1986)]; soils [Wu and Wang (1983); Wu and Sheu (1983); Wu *et al.* (1985); Wu and Aboutorabi (1988); Imai and Xie (1990)], ceramics [Wu *et al.* (1990)] and composite materials [Mathison *et al.* (1991)] were studied. Among other theoretical applications, the extension of the theory to finite deformation was made by Valanis (1977, 1978) by using the dual internal variables. Valanis and Fan (1983) applied the theory to study a non-homogeneous boundary value problem, that of a notch, with a demonstrated agreement by carefully conducted experiments on OHFC copper. Watanabe and Atluri (1985) proposed a new efficient scheme based upon their version of the theory with applications to a notched plate. Watanabe and Atluri (1986) used the new definition of intrinsic time to simulate the creep-plasticity behavior. Wu and Yeh (1988) revised the back stress and material function of the theory in order to describe the anisotropic hardening of the material behaviors. By

using the concept of corotational rate with the plastic spin, the theory was also applied to finite deformation by Im and Atluri (1987). Cases of finite uniaxial compression and torsion were discussed in their study. Wu *et al.* (1995) expressed the plastic spin in terms of the back stress and the rate-of-deformation tensors. In their investigation, the complex loading/unloading/reloading conditions were considered.

The kernel function of the theory is defined as a function of intrinsic time. It exhibits the weak singularity at the zero intrinsic time and is integrable in a finite domain. According to this mathematical characteristic, Valanis (1979, 1984) used a group of exponential decaying functions to form the kernel function. Thus, the constitutive equations of the theory could then be simplified into first-order ordinary differential constitutive equations. Murakami and Read (1989) investigated the performance of these equations with and without Richardson extrapolation. It was found that the extrapolation methods provide a significant increase in computational speed for comparable accuracy. Moreover, theoretical simulation of a uniaxial cyclic straining of annealed copper was shown to be close to the experimental data.

The viscoplastic behavior of material by using endochronic theory was first investigated by Wu and Yip (1980). The rate-sensitivity function of the intrinsic time measure was introduced for simulating the uniaxial strain-rate and its history effect. The uniaxial stress-strain responses of 1100-O aluminum and mild steel at various constant strain-rate conditions were theoretically discussed. Lin and Wu (1983) improved the rate-sensitivity function and investigated the material response under different strain-rate cases. Moreover, the derived constitutive equations were applied to the viscoplastic wave-propagation problem of a thin-walled tube subjected to impact loading. The rate-sensitivity functions, proposed by Wu and Yip (1980) and Lin and Wu (1983), are defined as a function of the uniaxial plastic strain-rate. The applicable region of the rate-sensitivity function is obviously restricted only to the uniaxial deformation. In their study, the total strain-rate was assumed to be approximately equal to the plastic strain-rate when the strain magnitude contains a greater degree of plastic strain. Based on this consideration, the rate-sensitivity function is a constant under certain constant strain-rate conditions.

To extend the theory in describing the viscoplastic behavior of material subjected to multiaxial loading, a new formulation of the rate-sensitivity function is presented in this study by using the equivalent plastic strain-rate. By considering the total strain-rate during the simulation process, the rate-sensitivity function is not a constant for certain constant strain-rate condition. Without neglecting the elastic part of the total strain-rate in the calculation, the stress–strain response for a small strain range or in transition area of the changing loading-direction can be properly described. In addition, the rate-sensitivity function proposed by Wu and Yip (1980) can be proved to be identical to the new formulation of the rate-sensitivity function for uniaxial loading.

An explicit numerical scheme proposed by Murakami and Read (1987, 1989) for integrating the first-order ordinary differential constitutive equations obtained by Valanis (1979, 1984) is adopted in this study. The constitutive equations for combined axial-torsional and biaxial loading cases are also derived. Experimental data for rate-independent behavior of OFHC copper tested by Lamba and Sidebottom (1978) are used for examining the theoretical simulation of the combined axial-torsional loading-path. The corresponding strain-paths are uniaxial cyclic straining and 90° out-of-phase loading with the prescribed circular strain. A satisfactory description is achieved by making a comparison with the experimental data. Next, viscoplastic behaviors of 304 stainless steel for uniaxial, combined axial-torsional and biaxial loading cases are investigated. Experimental data of uniaxial loading at different constant strain-rates or stress-rates, uniaxial loading with several-stepped change of strain-rate, combined axial-torsional strain-path under an elevated temperature of 650° and a square diamond shape of biaxial cyclic loading under strain-controlled condition tested by Yoshida (1989), Krempl (1979), Inoue *et al.* (1985) and Ellyin *et al.* (1991), respectively, are used for comparing with the endochronic simulation. It is shown, through comparison with the experimental results, that most of the viscoplastic behaviors of materials can be adequately simulated by endochronic theory with the newly proposed rate-sensitivity function.

2. THE ENDOCHRONIC THEORY

According to the condition of small deformation for homogeneous and isotropic materials, the deviatoric stress tensor **s** of endochronic constitutive is given by Valanis (1980):

$$\mathbf{s} = 2\int_0^z \rho(z-z')\frac{\partial \mathbf{e}^p}{\partial z'}\,dz' \tag{1}$$

where z is the intrinsic time scale, $\rho(z)$ is termed the kernel function and $\mathbf{e}^p$ is the deviatoric plastic strain tensor which is

$$d\mathbf{e}^p = d\mathbf{e} - \frac{d\mathbf{s}}{2\mu_0} \tag{2}$$

where **e** denotes the deviatoric strain tensor and μ_0 is the elastic shear modulus. The intrinsic time measure is

$$d\zeta = k\|d\mathbf{e}^p\| \quad \text{or} \quad d\zeta^2 = k^2\, d\mathbf{e}^p \cdot d\mathbf{e}^p \tag{3a,b}$$

in which $\|\cdot\|$ is the Euclidean norm and k is the rate-sensitivity function. The quantity of k is treated as unity for describing the material response of rate-independent effect. The material function (or hardening function) $f(\zeta)$ is

$$f(\zeta) = \frac{d\zeta}{dz} = 1 - Ce^{-\beta\zeta}, \quad \text{for } C < 1 \tag{4}$$

in which C and β are material parameters. The material function represents the effects of microstructural changes of material due to accumulation of the plastic strain history that is positive and satisfies the condition $f(0) = 1$. The material response of cyclic softening or hardening can be described by the value C. If the plastically incompressible is satisfied, the elastic hydrostatic response can be written as

$$d\sigma_{kk} = 3K\, d\varepsilon_{kk} \tag{5}$$

where σ_{kk} and ε_{kk} are the trace of stress and strain tensors and K is the elastic bulk modulus.

The kernel function $\rho(z)$ in eqn (1) is a weakly singular function at the original and integrable in the domain $0 \leqslant z \leqslant \infty$ [Valanis (1971)]. Valanis (1979, 1984) used a group of exponential decaying functions to form the kernel function, i.e.

$$\rho(z) = \sum_{r=1}^{n} C_r e^{-\alpha_r z}, \quad \rho(0) = \sum_{r=1}^{n} C_r \tag{6a,b}$$

in which C_r, α_r are parameters of material. Substitution of eqn (6a) into eqn (1) yields

$$\mathbf{s} = \sum_{r=1}^{n} \mathbf{s}_r \tag{7}$$

where

$$\mathbf{s}_r = 2\alpha_r \int_0^z e^{-\alpha_r(z-z')} \frac{\partial \mathbf{e}^p}{\partial z'} dz'. \tag{8}$$

According to the Leibnitz's differential rule, eqn (8) becomes the following linear first-order differential equations:

$$\frac{d\mathbf{s}_r}{dz} + \alpha_r \mathbf{s}_r = 2C_r \frac{d\mathbf{e}^p}{dz}, \quad r = 1, 2, \ldots, n \tag{9}$$

and

$$d\mathbf{s} = \sum_{r=1}^{n} d\mathbf{s}_r = 2\rho(0)\, d\mathbf{e}^p - \sum_{r=1}^{n} \alpha_r \mathbf{s}_r\, dz. \tag{10}$$

Substitution of eqn (2) into eqn (10) yields

$$d\mathbf{s} = \frac{\mu_0}{\mu_0 + \rho(0)} \left[2\rho(0)\, d\mathbf{e} - \sum_{r=1}^{n} \alpha_r \mathbf{s}_r\, dz \right]. \tag{11}$$

Using eqn (5), eqn (11) can be expressed in terms of the stress and strain tensors as

$$d\boldsymbol{\sigma} = p_1\, d\boldsymbol{\varepsilon} + p_2\, d\varepsilon_{kk}\mathbf{I} + p_3 \sum_{r=1}^{n} \alpha_r \left(\boldsymbol{\sigma} - \frac{\boldsymbol{\sigma}_{kk}}{3}\mathbf{I} \right)_r dz \tag{12}$$

where

$$p_1 = \frac{2\rho(0)}{1 + \dfrac{\rho(0)}{\mu_0}}, \quad p_2 = K - \frac{2\rho(0)}{3\left(1 + \dfrac{\rho(0)}{\mu_0}\right)}, \quad p_3 = \frac{-1}{1 + \dfrac{\rho(0)}{\mu_0}}. \tag{13a,b,c}$$

2.1. *Constitutive equations for combined axial-torsional loading case*

The stress and strain tensors for the combined axial-torsional loading of a thin-walled tube are

$$\boldsymbol{\sigma} = \begin{bmatrix} \sigma_1 & \tau & 0 \\ \tau & 0 & 0 \\ 0 & 0 & 0 \end{bmatrix}, \quad \boldsymbol{\varepsilon} = \begin{bmatrix} \varepsilon_1 & \eta & 0 \\ \eta & \varepsilon_2 & 0 \\ 0 & 0 & \varepsilon_2 \end{bmatrix} \tag{14a,b}$$

in which σ is the axial stress, τ is the shear stress, ε is the axial strain and η is the tensorial shear strain. The increment of the deviatoric plastic strain tensor $d\mathbf{e}^p$ becomes (eqn (2))

$$d\mathbf{e}^p = \begin{bmatrix} \dfrac{2}{3}(d\varepsilon_1 - d\varepsilon_2) - \dfrac{d\sigma_1}{3\mu_0} & d\eta - \dfrac{d\tau}{2\mu_0} & 0 \\ d\eta - \dfrac{d\tau}{2\mu_0} & -\dfrac{1}{3}(d\varepsilon_1 - d\varepsilon_2) + \dfrac{d\sigma_1}{6\mu_0} & 0 \\ 0 & 0 & -\dfrac{1}{3}(d\varepsilon_1 - d\varepsilon_2) + \dfrac{d\sigma_1}{6\mu_0} \end{bmatrix}. \tag{15}$$

Substitution of eqns (14a, b) into eqn (12) yields

$$d\sigma_1 = p_1\, d\varepsilon_1 + p_2(d\varepsilon_1 + 2\, d\varepsilon_2) + \frac{2}{3} p_3 \sum_{r=1}^{n} \alpha_r (\sigma_1)_r\, dz \tag{16}$$

$$d\sigma_2 = d\sigma_3 = p_1\, d\varepsilon_2 + p_2(d\varepsilon_1 + 2d\varepsilon_2) - \frac{1}{3} p_3 \sum_{r=1}^{n} \alpha_r (\sigma_1)_r\, dz = 0 \tag{17}$$

$$d\tau = p_1\, d\eta + p_3 \sum_{r=1}^{n} \alpha_r \tau_r\, dz \tag{18}$$

where the quantities of p_1, p_2 and p_3 are in eqns (13a–c). From eqn (17), one obtains

$$d\varepsilon_2 = A_1\, d\varepsilon_1 + A_2\, dz \tag{19}$$

where

$$A_1 = -\frac{p_2}{p_1 + 2p_2}, \quad A_2 = \frac{p_3}{3(p_1 + 2p_2)} \sum_{r=1}^{n} \alpha_r (\sigma_1)_r. \tag{20a,b}$$

Substitution of eqn (19) into eqn (16) leads to

$$d\sigma_1 = A_3\, d\varepsilon_1 + A_4\, dz \tag{21}$$

where

$$A_3 = p_1 + p_2 + 2p_2 A_1, \quad A_4 = 2p_2 A_2 + \frac{2}{3} p_3 \sum_{r=1}^{n} \alpha_r (\sigma_1)_r. \tag{22a,b}$$

Equation (18) can be written as

$$d\tau = p_1\, d\eta + A_5\, dz \tag{23}$$

where

$$A_5 = p_3 \sum_{r=1}^{n} \alpha_r \tau_r. \tag{24}$$

Substitution of eqns (4), (15), (19), (21) and (23) in eqn (3b) yields

$$\frac{f(\zeta)^2\, dz^2}{k^2} = (B_1\, d\varepsilon_1 + B_2\, dz)^2 + (B_3\, d\varepsilon_1 + B_4\, dz)^2 + (B_5\, d\eta + B_6\, dz)^2 \tag{25}$$

where

$$B_1 = \frac{2 - 2A_1}{3} - \frac{A_3}{3\mu_0} \tag{26}$$

$$B_2 = -\frac{2A_2}{3} - \frac{A_4}{3\mu_0} \tag{27}$$

$$B_3 = \frac{-4 + 4A_1}{3} + \frac{2A_3}{3\mu_0} \tag{28}$$

$$B_4 = \frac{4A_2}{3} + \frac{2A_4}{3\mu_0} \tag{29}$$

$$B_5 = 4 - \frac{2p_1}{\mu_0} \tag{30}$$

$$B_6 = -\frac{2A_5}{\mu_0}. \tag{31}$$

On rearrangement of eqn (25), the quadratic form with variable dz becomes

$$q_1\,dz^2 + q_2\,dz + q_3 = 0 \tag{32}$$

where

$$q_1 = B_2^2 + B_4^2 + B_6^2 - \frac{f(\zeta)^2}{k^2} \tag{33}$$

$$q_2 = 2(B_1B_2\,d\varepsilon_1 + B_3B_4\,d\varepsilon_1 + B_5B_6\,d\eta) \tag{34}$$

$$q_3 = B_1^2\,d\varepsilon_1^2 + B_3^2\,d\varepsilon_1^2 + B_5^2\,d\eta^2. \tag{35}$$

The increment of the intrinsic time scale dz is calculated to be

$$dz = \frac{-q_2 \pm \sqrt{q_2^2 - 4q_1q_3}}{2q_1}. \tag{36}$$

By definition, the intrinsic time measure ζ in eqn (3a) is invariably greater than or equal to zero. The expression of $d\zeta$ in eqn (3b) is expected to generate two roots of the opposite sign or zero value [Murakami and Read (1987, 1989)]. The material function, as shown in eqn (4), invariably exceeds zero. Therefore, two roots of opposite sign or zero value are found in eqn (36), the positive root is the desired one.

The differential increments $d\varepsilon_1$ and $d\eta$ are considered here to be the input value. The parameters $A_1, \ldots, A_6$, $B_1, \ldots, B_6$, q_1, q_2 and q_3 are determined according to the known values of ζ, z, ε_1, η, σ_1 and τ at the current state of loading. The increment of the intrinsic time scale dz is determined from eqn (36). Consequently, the incremental quantities $d\zeta$, $d\varepsilon_2$, $d\sigma_1$ and $d\tau$ are obtained from eqns (4), (19), (21) and (23), respectively. The loading process can be readily completed by repeatedly updating the values of ζ, z, ε_1, η, σ_1 and τ during the calculation.

2.2. *Constitutive equations for biaxial loading case*

The stress and strain tensors in the case of biaxial loading are

$$\boldsymbol{\sigma} = \begin{bmatrix} \sigma_1 & 0 & 0 \\ 0 & \sigma_2 & 0 \\ 0 & 0 & 0 \end{bmatrix} \quad \boldsymbol{\varepsilon} = \begin{bmatrix} \varepsilon_1 & 0 & 0 \\ 0 & \varepsilon_2 & 0 \\ 0 & 0 & \varepsilon_3 \end{bmatrix}. \tag{37a,b}$$

The increment of the deviatoric plastic strain tensor $d\mathbf{e}^p$ from eqn (2) is

$$\mathrm{d}\mathbf{e}^{\mathrm{p}} = \begin{bmatrix} \dfrac{2\,\mathrm{d}\varepsilon_1 - \mathrm{d}\varepsilon_2 - \mathrm{d}\varepsilon_3}{3} - \dfrac{2\,\mathrm{d}\sigma_1 - \mathrm{d}\sigma_2}{6\mu_0} & 0 & \\ 0 & \dfrac{2\,\mathrm{d}\varepsilon_2 - \mathrm{d}\varepsilon_1 - \mathrm{d}\varepsilon_3}{3} - \dfrac{2\,\mathrm{d}\sigma_2 - \mathrm{d}\sigma_1}{6\mu_0} & \\ 0 & 0 & \end{bmatrix} \times \begin{bmatrix} 0 \\ 0 \\ \dfrac{2\,\mathrm{d}\varepsilon_3 - \mathrm{d}\varepsilon_1 - \mathrm{d}\varepsilon_2}{3} + \dfrac{\mathrm{d}\sigma_1 + \mathrm{d}\sigma_2}{6\mu_0} \end{bmatrix}. \tag{38}$$

Substitution of eqns (37a, b) into eqn (12) yields

$$\mathrm{d}\sigma_1 = p_1\,\mathrm{d}\varepsilon_1 + p_2(\mathrm{d}\varepsilon_1 + \mathrm{d}\varepsilon_2 + \mathrm{d}\varepsilon_3) + p_3 \sum_{r=1}^{3} \alpha_r \left(\frac{2\sigma_1 - \sigma_2}{3}\right)_r \mathrm{d}z \tag{39}$$

$$\mathrm{d}\sigma_2 = p_1\,\mathrm{d}\varepsilon_2 + p_2(\mathrm{d}\varepsilon_1 + \mathrm{d}\varepsilon_2 + \mathrm{d}\varepsilon_3) + p_3 \sum_{r=1}^{n} \alpha_r \left(\frac{2\sigma_2 - \sigma_1}{3}\right)_r \mathrm{d}z \tag{40}$$

$$\mathrm{d}\sigma_3 = p_1\,\mathrm{d}\varepsilon_3 + p_2(\mathrm{d}\varepsilon_1 + \mathrm{d}\varepsilon_2 + \mathrm{d}\varepsilon_3) - p_3 \sum_{r=1}^{n} \alpha_r \left(\frac{\sigma_1 + \sigma_2}{3}\right)_r \mathrm{d}z = 0. \tag{41}$$

From eqn (41), one obtains

$$\mathrm{d}\varepsilon_3 = C_1\,\mathrm{d}\varepsilon_1 + C_1\,\mathrm{d}\varepsilon_2 + C_2\,\mathrm{d}z \tag{42}$$

where

$$C_1 = \frac{-p_2}{p_1 + p_2}, \quad C_2 = \frac{p_3}{p_1 + p_2} \sum_{r=1}^{n} \alpha_r \left(\frac{\sigma_1 + \sigma_2}{3}\right)_r. \tag{43a,b}$$

Substitution of eqn (42) into eqns (39) and (40) leads to

$$\mathrm{d}\sigma_1 = C_3\,\mathrm{d}\varepsilon_1 + C_4\,\mathrm{d}\varepsilon_2 + C_5\,\mathrm{d}z \tag{44}$$

and

$$\mathrm{d}\sigma_2 = C_4\,\mathrm{d}\varepsilon_1 + C_3\,\mathrm{d}\varepsilon_2 + C_6\,\mathrm{d}z \tag{45}$$

where

$$\begin{aligned} C_3 &= p_1 + p_2 + p_2 C_1 \\ C_4 &= p_2 + p_2 C_1 \\ C_5 &= p_2 C_2 + p_3 \sum_{r=1}^{n} \alpha_r \left(\frac{2\sigma_1 - \sigma_2}{3}\right)_r \\ C_6 &= p_2 C_2 + p_3 \sum_{r=1}^{n} \alpha_r \left(\frac{2\sigma_2 - \sigma_1}{3}\right)_r. \end{aligned} \tag{46a,b,c,d}$$

By substituting eqns (4), (38), (42), (44) and (45) in eqn (3b), a quadratic form with variable dz, which is similar to eqn (32), is determined. Again, the differential increments $d\varepsilon_1$ and $d\varepsilon_2$ are considered to be the input values for biaxial loading. Since the parameters are determined from the known values of ζ, z, ε_1, ε_2, σ_1 and σ_2 at the current state of loading, the increment of the intrinsic time scale dz can be found from the quadratic equation. The incremental quantities $d\zeta$, $d\varepsilon_3$, $d\sigma_1$ and $d\sigma_2$ are obtained from eqns (4), (42), (44) and (45), respectively. Thus, the loading process can be easily determined by repeatedly updating the values of ζ, z, ε_1, ε_2, σ_1 and σ_2 during the calculation.

3. RATE-SENSITIVITY FUNCTION

The endochronic theory for elastic-plastic deformation was first proposed by Valanis (1971). The intrinsic time measure was defined in terms of the total strain tensor. Lin and Wu (1976) introduced a rate-sensitivity function, which is a function of total strain-rate, and applied the function to describe the viscoplastic behavior of material for the uniaxial strain-rate effect. Due to the discrepancy between the theoretical and experimental results in case of unloading, Valanis (1980) redefined the definition of the intrinsic time measure by plastic strain tensor. Based on this new definition, Wu and Yip (1980) proposed a new formulation of the rate-sensitivity function by the deviatoric plastic strain-rate. The function has been used in describing the viscoplastic behavior of material for the case of uniaxial strain-rate and its history effect. The rate-sensitivity function is

$$k(\dot{e}_1^p) = 1 - k_a \log\left[\frac{\dot{e}_1^p}{(\dot{e}_1^p)_0}\right] \tag{47}$$

where $(\dot{e}_1^p)_0$ is the reference uniaxial deviatoric plastic strain-rate, $\dot{e}_1^p$ is the relative uniaxial deviatoric plastic strain-rate and k_a is a rate-sensitivity parameter. Lin and Wu (1983) modified the formulation of rate-sensitivity function to be

$$k(\dot{e}_1^p) = 1 - k_a \log\left[\frac{\dot{e}_1^p}{(\dot{e}_1^p)_0}\right] - k_b \log\left[\frac{\dot{e}_1^p}{(\dot{e}_1^p)_0}\right]^2 \tag{48}$$

where k_b is the second-order rate-sensitivity parameter. This form of the rate-sensitivity function was applied to investigate the viscoplastic wave-propagation problem of a thin-walled tube subjected to impact loading. It seems apparent that the applicable region of the rate-sensitivity functions in both eqns (47) and (48) is restricted only to uniaxial deformation. In addition, the plastic strain-rate was considered in their study to be equal to the total strain-rate in the large strain range, therefore, the value of rate-sensitivity function k is a constant for a certain fixed strain-rate condition. However, if the elastic part of the strain-rate is neglected, a significant discrepancy between the theoretical simulation and experimental data may occur for a small strain range. Furthermore, if the above situation is considered for multiaxial loading, the same drawback of the theoretical simulation at the transition area may occur when the loading direction is altered. Therefore, a new formulation of the rate-sensitivity function is proposed for the case of multiaxial loading, i.e.

$$k = 1 - k_a \log\left[\frac{\dot{e}_{eq}^p}{(\dot{e}_{eq}^p)_0}\right] \tag{49}$$

where $(\dot{e}_{eq}^p)_0$ is the reference equivalent deviatoric plastic strain-rate and $\dot{e}_{eq}^p$ is the relative equivalent deviatoric plastic strain-rate. They are defined to be

$$(\dot{e}^{p}_{eq})_0 = \sqrt{\tfrac{2}{3}(\dot{\mathbf{e}}^{p})_0 \cdot (\dot{\mathbf{e}}^{p})_0} \tag{50}$$

and

$$\dot{e}^{p}_{eq} = \sqrt{\tfrac{2}{3}\dot{\mathbf{e}}^{p} \cdot \dot{\mathbf{e}}^{p}} \tag{51}$$

where $(\dot{\mathbf{e}}^{p})_0$ is the reference deviatoric plastic strain-rate tensor and $\dot{\mathbf{e}}^{p}$ is the relative deviatoric plastic strain-rate tensor. Notably, the total strain-rate is considered in the theoretical simulation, the rate-sensitivity function k is a changeable value during the calculation.

3.1. *Relationship between the newly proposed rate-sensitivity function and the rate-sensitivity function proposed by Wu and Yip* (1980)

If a material is assumed to be plastically incompressible, the plastic strain-rate tensor $\dot{\boldsymbol{\varepsilon}}^{p}$ and deviatoric plastic strain-rate tensor $\dot{\mathbf{e}}^{p}$ for uniaxial loading are

$$\dot{\boldsymbol{\varepsilon}}^{p} = \dot{\mathbf{e}}^{p} = \begin{bmatrix} \dot{\varepsilon}^{p}_1 & 0 & 0 \\ 0 & -0.5\dot{\varepsilon}^{p}_1 & 0 \\ 0 & 0 & -0.5\dot{\varepsilon}^{p}_1 \end{bmatrix} \tag{52a,b}$$

where $\dot{\varepsilon}^{p}$ is the uniaxial plastic strain-rate. The quantities of $(\dot{e}^{p}_{eq})_0$ and $\dot{e}^{p}_{eq}$ are determined from eqns (50) and (51) to be

$$(\dot{e}^{p}_{eq})_0 = \sqrt{\tfrac{2}{3}\{(\dot{\varepsilon}^{p}_1)^2_0 + 2[-0.5(\dot{\varepsilon}^{p}_1)_0]^2\}} = (\dot{\varepsilon}^{p}_1)_0 \tag{53}$$

and

$$\dot{e}^{p}_{eq} = \dot{\varepsilon}^{p}_1. \tag{54}$$

Substitution of eqns (53) and (54) into (49) leads to

$$k = 1 - k_a \log\left[\frac{\dot{\varepsilon}^{p}_1}{(\dot{\varepsilon}^{p}_1)_0}\right]. \tag{55}$$

It is shown that the result from eqn (55) is identical to the result obtained from eqn (47) for uniaxial loading. However, the formulation of eqn (49) can be used for simulating the viscoplastic behavior of material under multiaxial loading.

3.2. *Calculation of the rate-sensitivity function for uniaxial loading under constant strain-rates*

The differential increment of the uniaxial strain $d\varepsilon$ is considered to be the incremental step, which is a known quantity. Figure 1 shows the schematic drawing of the uniaxial

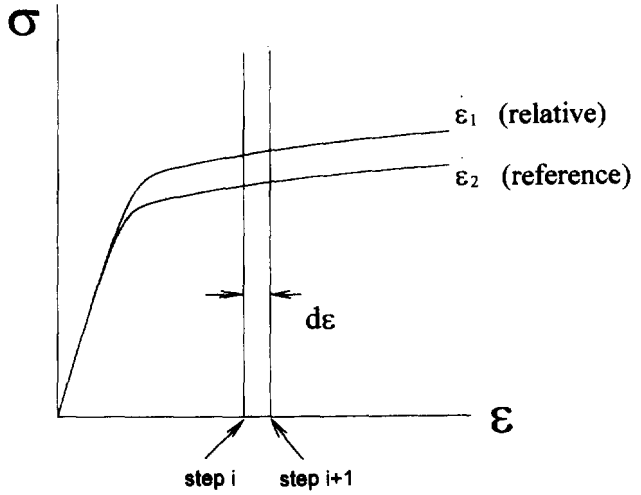

Fig. 1. Schematic drawing of uniaxial stress–strain curves for two different constant strain-rates.

stress-strain curve for two different constant strain-rates. The lower curve is denoted as the reference curve and the higher curve is the relative curve. The increments of time for reference and relative curves from step i to step $i+1$ are

$$(\mathrm{d}t)_0 = \frac{\mathrm{d}\varepsilon}{(\dot{\varepsilon})_0}, \quad \mathrm{d}t = \frac{\mathrm{d}\varepsilon}{\dot{\varepsilon}}. \tag{56a,b}$$

The quantities of the stress, strain and value of the rate-sensitivity function are assumed here to be known for the reference and relative curves at step i. Note that the value of the rate-sensitivity function for reference curve is always one. Next, the amount of the rate-sensitivity function of the relative curve at step $i+1$ is determined on the basis of the known quantities at step i. The deviatoric plastic strain increment $(\mathrm{d}\mathbf{e}^{\mathrm{p}})_0$ of reference curve and deviatoric plastic strain increment $\mathrm{d}\mathbf{e}^{\mathrm{p}}$ of relative curve for step $i+1$ are calculated by using the endochronic theory. Using eqns (56a, b), the deviatoric plastic strain-rate $(\dot{\mathbf{e}}^{\mathrm{p}})_0$ of the reference curve and deviatoric plastic strain-rate $\dot{\mathbf{e}}^{\mathrm{p}}$ of the relative curve are determined to be

$$(\dot{\mathbf{e}}^{\mathrm{p}})_0 = \frac{(\mathrm{d}\mathbf{e}^{\mathrm{p}})_0}{(\mathrm{d}t)_0}, \quad \dot{\mathbf{e}}^{\mathrm{p}} = \frac{\mathrm{d}\mathbf{e}^{\mathrm{p}}}{\mathrm{d}t}. \tag{57a,b}$$

Substituting eqns (57a,b) into eqns (50) and (51), the equivalent deviatoric strain-rate $(\dot{e}^{\mathrm{p}}_{\mathrm{eq}})_0$ for the reference curve and the equivalent deviatoric plastic strain-rate $\dot{e}^{\mathrm{p}}_{\mathrm{eq}}$ for the relative curve for step $i+1$ are determined. Consequently, the amount of rate-sensitivity function k for step $i+1$ is obtained from eqn (49).

3.3. *Calculation of the rate-sensitivity function for uniaxial loading under constant strain-rates and stress-rates*

A constant stress-rate case is assumed here to be the relative curve for uniaxial loading and an uniaxial constant strain-rate case is the reference curve. Again, the differential increment of the strain $\mathrm{d}\varepsilon$ is considered to be a known incremental step. By using the known values of the stress, strain and rate-sensitivity function at step i, the quantities $\mathrm{d}\mathbf{e}^{\mathrm{p}}$ and increment of the uniaxial stress $\mathrm{d}\sigma$ of the relative curve for step $i+1$ are determined by endochronic theory. The increment of time for the relative curve from step i to step $i+1$ is

$$\mathrm{d}t = \frac{\mathrm{d}\sigma}{\dot{\sigma}}. \tag{58}$$

The deviatoric plastic strain-rate $\dot{\mathbf{e}}^{\mathrm{p}}$ of relative curve is determined from eqn (57b). The deviatoric plastic strain-rate $(\mathbf{e}^{\mathrm{p}})_0$ of the reference curve is obtained from Section 3.2. The amount of rate-sensitivity function k for the relative curve at step $i+1$ is easily obtained by using the eqns (50), (51) and (49).

3.4. *Calculation of the rate-sensitivity function for multiaxial loading under constant strain-rates*

Next, a multiaxial strain-path with a constant strain-rate is assumed here to be the relative path, and an uniaxial loading with a constant strain-rate is the reference curve. The strain-rate for the multiaxial strain-path is denoted as $\dot{L}$. The differential incremental step of the uniaxial strain $\mathrm{d}\varepsilon$ is allowed to be equal to the incremental length of the multiaxial strain-path $\mathrm{d}L$, which is defined as

$$\mathrm{d}L = \sqrt{\mathrm{d}\boldsymbol{\varepsilon} \cdot \mathrm{d}\boldsymbol{\varepsilon}}. \tag{59}$$

The quantities of the components of stress and strain and the value of the rate-sensitivity function are assumed here to be known for the relative path at step i. The deviatoric plastic

strain increment $d\mathbf{e}^p$ of relative path for step $i+1$ is calculated by using the endochronic theory. The increment of time for relative path from step i to step $i+1$ is

$$dt = \frac{dL}{\bar{L}}. \tag{60}$$

The deviatoric plastic strain-rate $\dot{\mathbf{e}}^p$ of relative path is determined from eqn (57b). The deviatoric plastic strain-rate $(\mathbf{e}^p)_0$ of the reference curve is obtained from Section 3.2. The amount of rate-sensitivity function k for step $i+1$ is obtained by using the eqns (50), (51) and (49). Notably, experimental data indicate that the stress-strain curves with different stress-rates or strain-rates coincide at the initial loading range. Therefore, the initial value of the rate-sensitivity function for relative curve is treated to be one.

4. COMPARISON AND DISCUSSION OF THE THEORETICAL AND EXPERIMENTAL RESULTS

In this section, theoretical results are compared with experimental data obtained by Lamba and Sidebottom (1978), Krempl (1979), Inoue *et al.* (1985), Yoshida (1989) and Ellyin *et al.* (1991). Tested materials include OFHC copper for rate-independent response and 304 stainless steel (at room temperature or elevated temperature) for viscoplastic response. Parameters of the materials for the theory are determined according to the method proposed by Fan (1983). Material behaviors of 304 stainless steel tested by Krempl (1979) and Yoshida (1989) are similar; a group of material parameters is used for theoretical simulation. However, the material responses of 304 stainless steel tested by Krempl (1979) and Ellyin *et al.* (1991) are quite different, as indicated from the uniaxial yield strengths for both experiments. Therefore, another group of material parameters is required to be found. The same material tested by Inoue *et al.* (1985) is conducted under an elevated temperature of 650°. The material response is also different from the material response tested by Krempl (1979) and Ellyin *et al.* (1991). Thus, a different group of material parameters is also necessary to be calculated. Table 1 lists the material parameters for OFHC copper and 304 stainless steel.

4.1. *Stress-strain response of OFHC copper for rate-independent effect*

The experimental result of uniaxial cyclic stress-strain curve for OFHC copper tested by Lamba and Sidebottom (1978) is shown in Fig. 2(a). Figure 2(b) shows the simulated result obtained by endochronic theory. Due to the rate-independent behavior, the parameter k_a of the rate-sensitivity function is treated as zero. The strain-path of the 90° out-of-phase loading with the prescribed circular effective strain amplitude $\Delta\bar{\varepsilon} = 1\%$ beginning with axial loading is shown in Fig. 3. Figure 4(a) shows the experimental cyclic axial-shear stress curve. The figure indicates that, after drastic cyclic hardening, the stress loop is stabilized in the 10th cycle. Figure 4(b) is the corresponding simulated result. The experimental and theoretical results of the axial stress-strain curve are shown in Figs 5(a, b). The corresponding experimental and theoretical results of the shear stress–strain curve are shown in Figs 6(a, b). These figures confirm that the theoretical prediction correlates well with the experimental result.

4.2. *Uniaxial cyclic stress–strain responses of* 304 *stainless steel for viscoplastic effect*

The experimental data of uniaxial stress-strain curves at different constant strain-rates or constant stress-rate for 304 stainless steel tested by Yoshida (1989) is summarized in Fig. 7. In their test, the constant strain-rates were controlled to be $10^{-2}\ s^{-1}$ and $10^{-6}\ s^{-1}$, and the constant stress-rate was 30 MPa s^{-1}. The theoretical simulation by endochronic theory is also shown in Fig. 7. Krempl (1979) tested 304 stainless steel for uniaxial stress–strain response of several-stepped changes of the strain-rate. Figure 8 shows the experimental and theoretical stress-strain curves of three tensile tests at strain-rates ranging from 10^{-2} to $10^{-8}\ s^{-1}$. In two of the tests, the strain-rate was instantaneously changed by three orders of magnitude at points A. The response of a cyclically saturated specimen to repeated

Table 1. Material parameters for OFHC copper and 304 stainless steel

	μ_0 (MPa)	K (MPa)	C_1 (MPa)	C_2 (MPa)	C_3 (MPa)	α_1	α_2	α_3	C	β	k_a
OFHC Copper (Lambda)	33100	83265	4.2×10^5	5.2×10^3	1.2×10^3	8860	500	110	0.7	10.2	0
304 stainless steel (Krempl and Yoshida)	69579	181373	6.1×10^5	4.1×10^3	8×10^2	7800	350	70	0.33	10.2	0.0537
304 stainless steel (Inoue)	42667	112022	5.6×10^5	6.95×10^3	1.6×10^3	7680	510	110	0.235	9.2	0.0424
304 stainless steel (Ellyin)	70769	153333	6.12×10^5	4.1×10^3	8×10^3	7350	580	175	0.33	9.0	0.0507

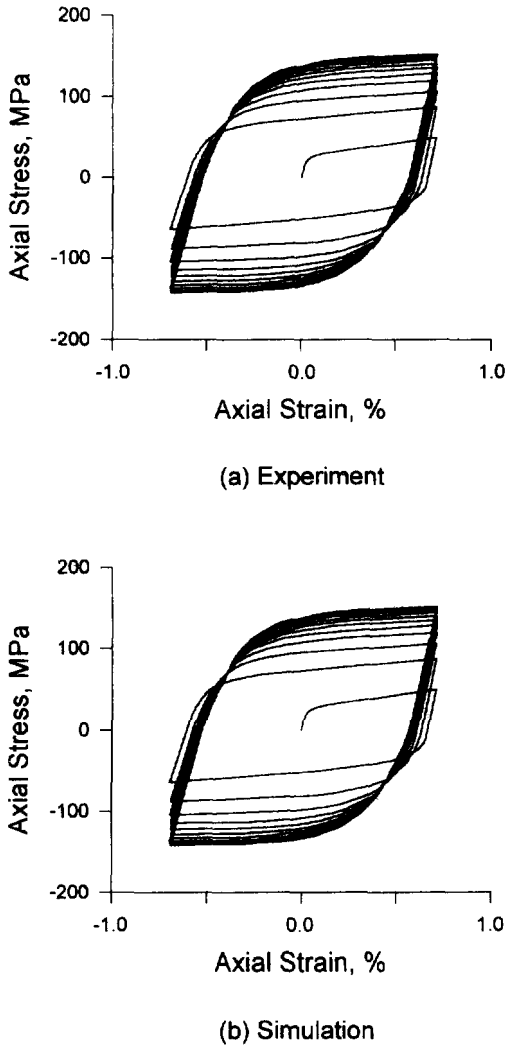

Fig. 2. Experimental and theoretical stress–strain curves for OHFC copper under uniaxial cyclic straining.

strain-rate changes was reported by Krempl (1979) and is shown in Fig. 9. The specimen was subjected to completely reversed cycling at $\pm 0.4\%$ until the cyclic steady-state was reached. Next, the specimen was tested with sudden changes in strain-rate between the value of 10^{-3}–$10^{-5}\,s^{-1}$. Experimental and theoretical results of the material behaviors under cyclic loading and repeated strain-rate changes are depicted in Figs 10(a, b), respectively. At the strain of $\pm 0.2\%$, the strain-rate was switched between 10^{-3} to $10^{-5}\,s^{-1}$.

Thin-walled circular cylindrical specimens of stainless steel type 304, as tested by Ellyin *et al.* (1991), were subjected to uniaxial cyclic loading under a strain-controlled condition. Each test comprised of three levels of strain-rates applied in a predetermined order. In each step, 50 cycles were applied before switching to another one in order to ensure stable response at each strain-rate level. The controlled strain amplitude was $\Delta\varepsilon = \pm 0.3\%$ with strain-rates ranging from 6×10^{-3} to 6×10^{-4} to $6 \times 10^{-5}\,s^{-1}$. Figure 11 shows the experimental and theoretical results of the stress amplitude vs number of cycles for uniaxial cyclic loading. The figure indicates that after transient cyclic hardening occurs during a few initial cycles, the stress–strain response is stabilized. However, an abrupt change in the size of the stress–strain loop occurs when a different strain-rate is applied. Notably, the endochronic theory with the newly proposed rate-sensitivity function simulates fairly well the characteristic behavior of the material to the abrupt changes of strain-rate.

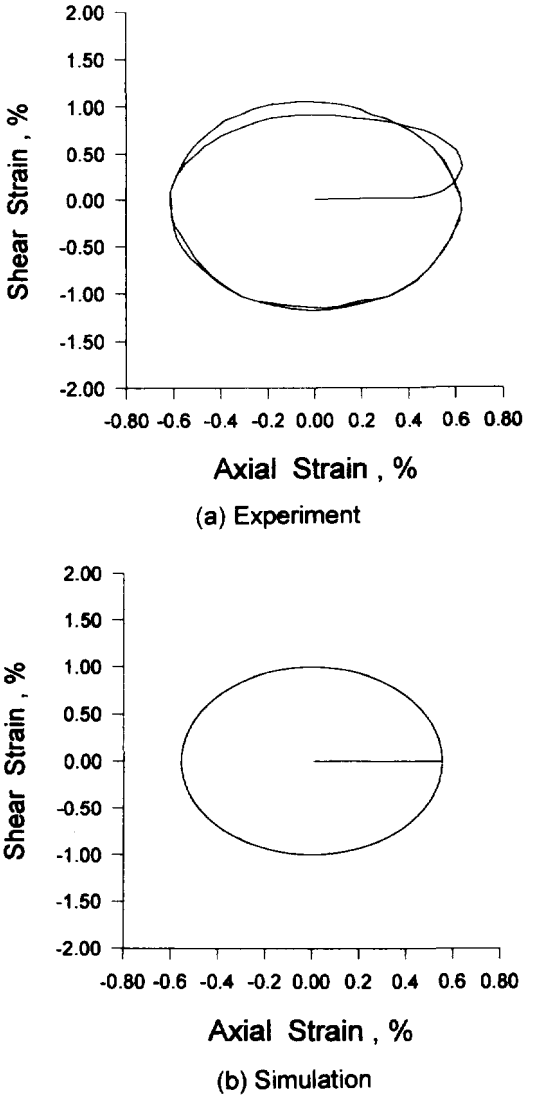

Fig. 3. Experimental and theoretical trajectories of 90° out-of-phase strain path for OHFC copper with the prescribed circular effective strain amplitude $\Delta\bar{\varepsilon} = 1\%$.

4.3. *Combined axial-torsional stress–strain responses of* 304 *stainless steel for viscoplastic effect*

Experimental data of 304 stainless steel under an elevated temperature of 650° for combined axial-torsional strain-path were tested by Inoue *et al.* (1985). A schematic drawing of the strain trajectory is shown in Fig. 12. It is shown that a proportional strain-path in 45° direction was denoted as Stage I, followed by Stage II, in which the ratio of the strain-rate was $\dot{\varepsilon}/(\dot{\gamma}/\sqrt{3}) = 5$. Subsequently, the direction of the strain-path in Stage III changed to the same as in Stage I. Two kinds of equivalent strain-rates were selected to investigate the effect of the strain-rate, as shown in the inset table of Fig. 12. Figure 13 demonstrates the experimental and theoretical results of the axial stress–strain curve for HHH loading case. The corresponding shear stress–strain and equivalent stress–strain curves are depicted in Figs 14 and 15. Figure 16 shows the experimental and theoretical results of the axial stress–strain curve for LHL loading case. The corresponding shear stress–strain and equivalent stress–strain curves are depicted in Figs 17 and 18. The cumulated axial deformation due to the mechanical ratcheting was investigated by Inoue *et al.* (1985). The cyclic torsional strain range $\Delta\gamma/\sqrt{3}$ was 1.5% when the axial stress ($\sigma = 67$ MPa) was kept constant. Two strain-rates, $\dot{\gamma}/\sqrt{3} = 0.1\%\ \text{s}^{-1}$ and $\dot{\gamma}/\sqrt{3} = 0.002\%\ \text{s}^{-1}$, were selected for investigation. The controlled strain-path is shown in Fig. 19. Figures 20 and 21 show the experimental

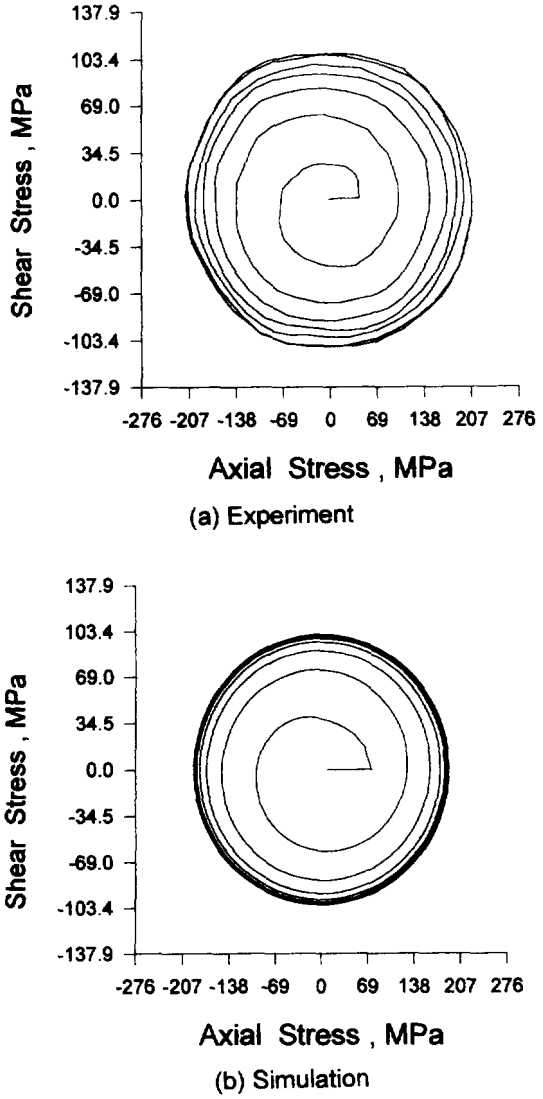

Fig. 4. Experimental and theoretical axial-shear stress curves for OHFC copper under the loading condition of 90° out-of-phase strain path.

and theoretical axial strain vs shear strain curves for two strain-rate cases. Notably, the theoretical simulations correlate well with the experimental findings.

4.4. *Biaxial stress–strain responses of* 304 *stainless steel for viscoplastic effect*

Ellyin *et al.* (1991) tested the thin-walled circular cylindrical specimens of stainless steel type 304 subjected to biaxial cyclic loading under a strain-controlled condition. The strain-path for the biaxial cyclic loading is shown in Fig. 22. The material is initially loaded to point A and, subsequently, the cyclic loading-path follows a square-diamond shape ABCDA. Figure 23(a) shows the axial stress–strain curve for the first 10 cycles at a strain-rate of $4 \times 10^{-3}\,s^{-1}$. A transient stress–strain response is observed during a few initial cycles. Figure 23(b) is the simulated results of the axial stress–strain response. Although the predicted stress–strain curve for first few cycles is slightly different from the experimental observation, the stable stress–strain loop is very close to experimental data. The corresponding experimental and theoretical results of the tangential stress–strain curve are shown in Figs 24(a, b). The experimental and theoretical results of the tangential stress and axial stress curve are shown in Figs 25(a, b). A comparison with the experimental data reveals that most of the viscoplastic behaviors of materials can be adequately simulated by endochronic theory with the newly proposed rate-sensitivity function.

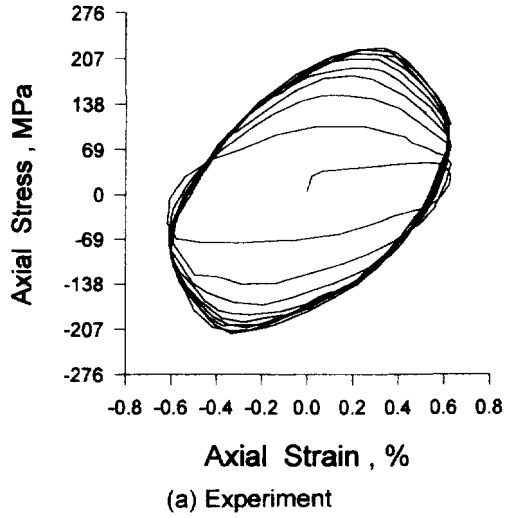

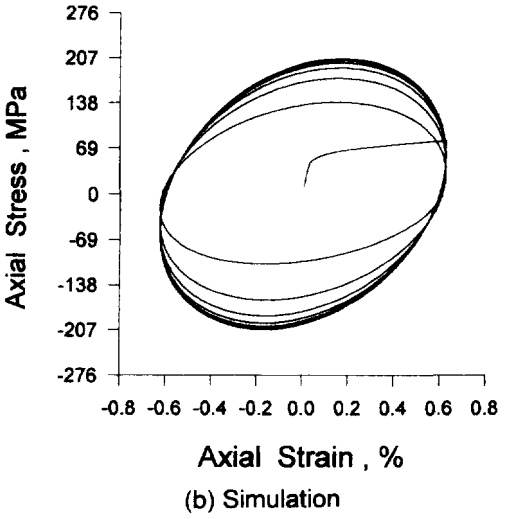

Fig. 5. Experimental and theoretical axial stress–strain curves for OHFC copper under the loading condition of 90° out-of-phase strain path.

5. CONCLUSIONS

In this paper, the first-order differential equations, which were obtained by Valanis (1979, 1984), are extended to describe the response of materials under various strain-paths in a multi-dimensional strain space. Explicit constitutive equations for combined axial-torsional and biaxial loading cases are divided. A strain-path of the 90° out-of-phase loading with the prescribed circular effective strain beginning with axial loading of OFHC copper for rate-independent effect is investigated. Theoretical prediction correlates well with the experimental result.

A rate-sensitivity function, which is defined by equivalent plastic strain-rate, is presented in this paper. It is proved that the rate-sensitivity function introduced by Wu and Yip (1980) is identical to the newly proposed rate-sensitivity function for uniaxial loading. However, the new formulation of the rate-sensitivity function can be used in endochronic theory for simulating the viscoplastic response of material under multiaxial loading. In our study, several cases of uniaxial loading, combined axial-torsional loading and biaxial loading with various strain-rate or stress-rate cases for stainless steel are included. It is shown that the theoretical simulations are in good agreement with the experimental data.

Acknowledgement—The work presented was carried out with the support of National Science Council under grant NSC 84-2212-E-006-043. Its support is gratefully acknowledged.

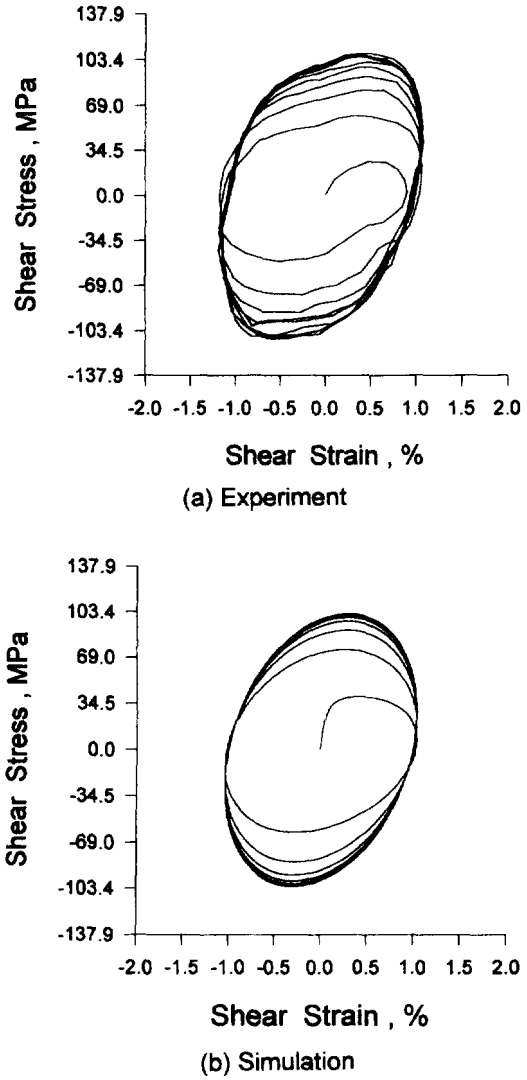

Fig. 6. Experimental and theoretical shear stress–strain curves for OHFC copper under the loading condition of 90° out-of-phase strain path.

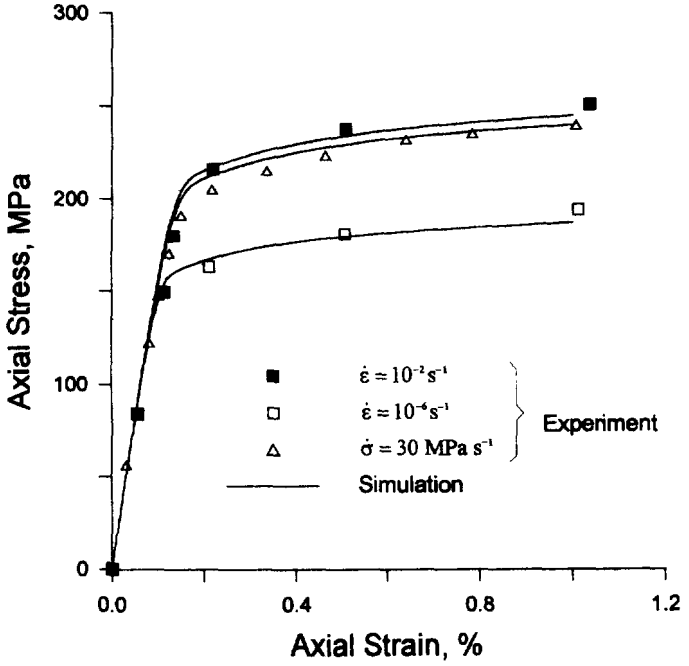

Fig. 7. Experimental and theoretical uniaxial stress–strain curves for 304 stainless steel at different constant strain-rates or constant stress rate.

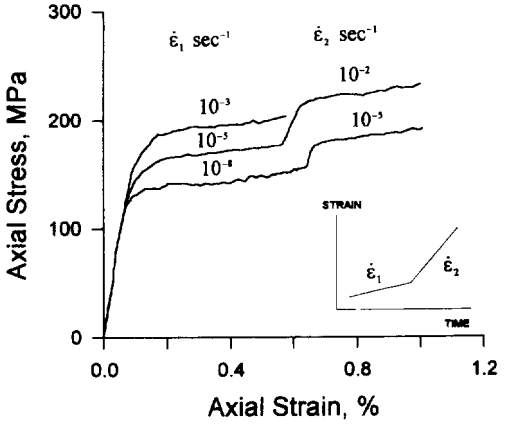

(a) Experiment

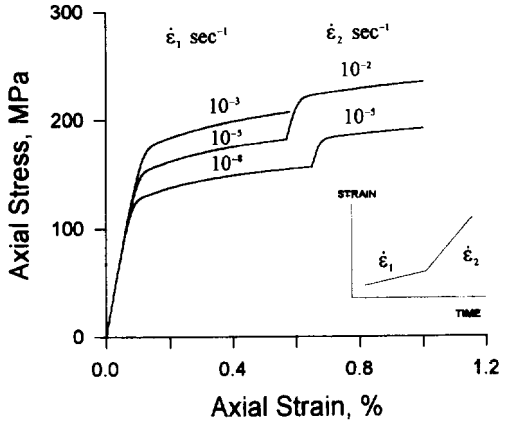

(b) Simulation

Fig. 8. Experimental and theoretical uniaxial stress–strain curves for 304 stainless steel at strain-rates ranging from 10^{-2} to 10^{-8} s^{-1}.

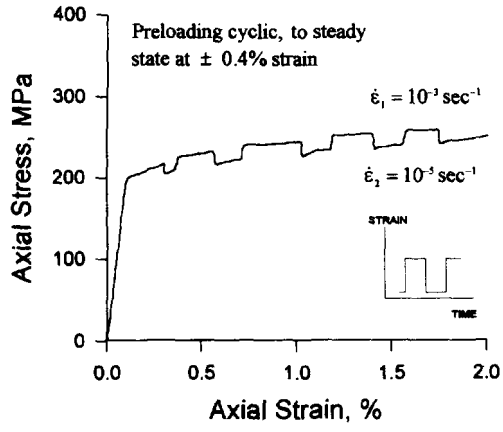

(a) Experiment

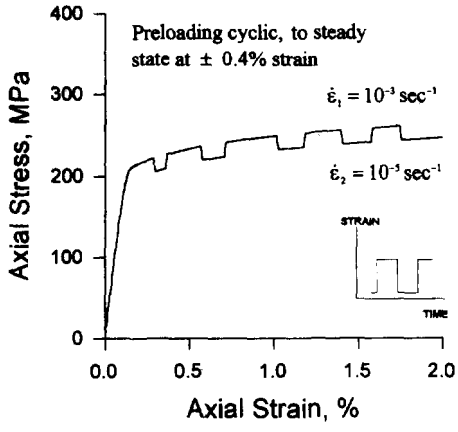

(b) Simulation

Fig. 9. Experimental and theoretical responses of a cyclically saturated specimen for 304 stainless steel under the loading condition of repeated strain-rate changes.

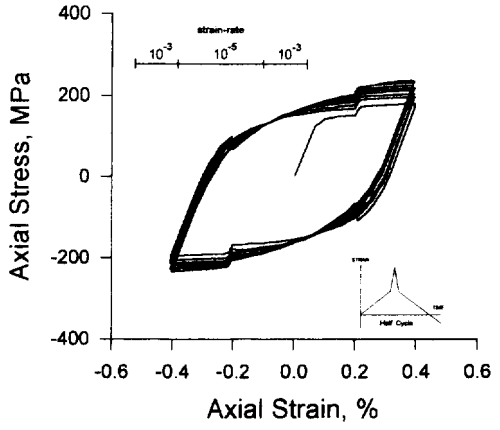

(a) Experiment

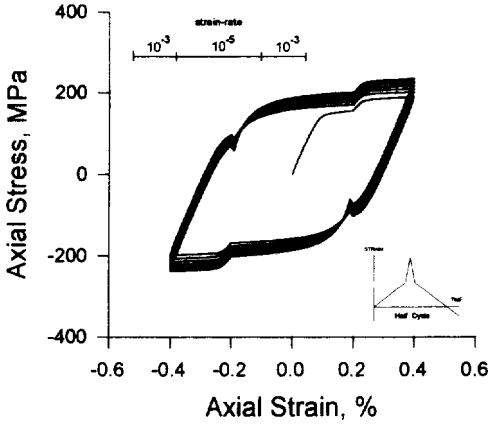

(b) Simulation

Fig. 10. Experimental and theoretical uniaxial stress–strain curves for 304 stainless steel under cyclic loading and repeated strain-rate changes.

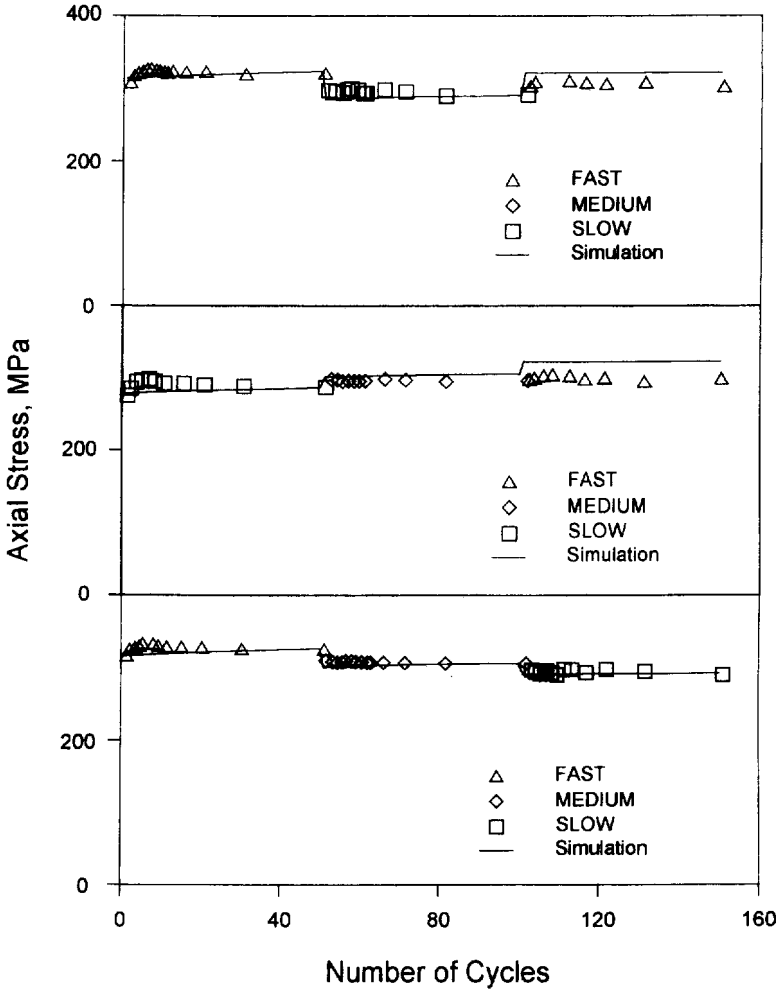

Fig. 11. Experimental and theoretical results of the stress amplitude vs number of cycles for 304 stainless steel under uniaxial cyclic loading.

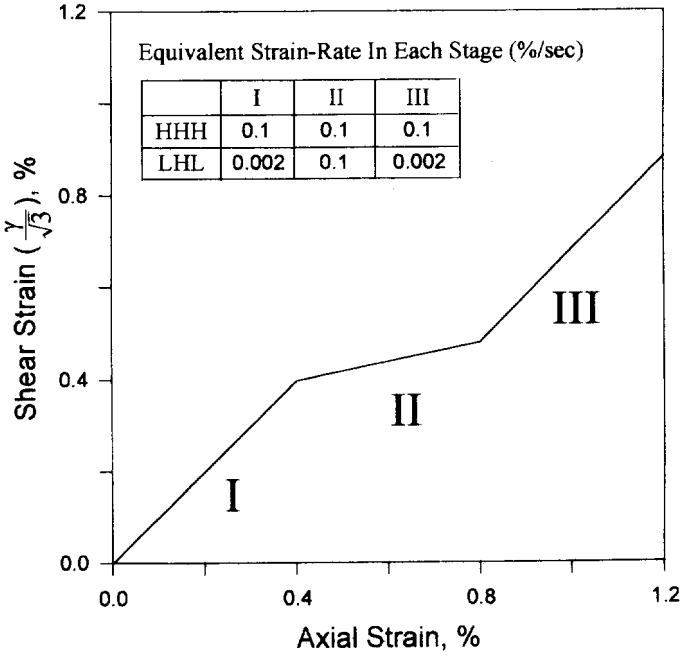

Fig. 12. A schematic drawing of the strain trajectory for 304 stainless steel tested by Inoue *et al.* (1985).

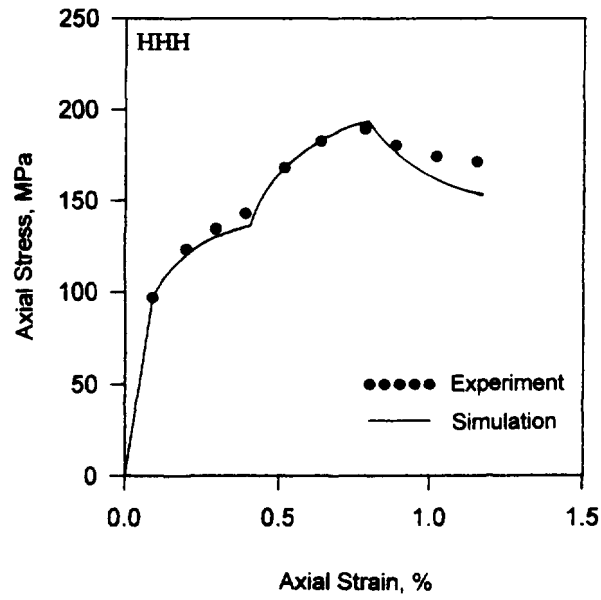

Fig. 13. Experimental and theoretical results of the axial stress–strain curve for 304 stainless steel under HHH loading condition.

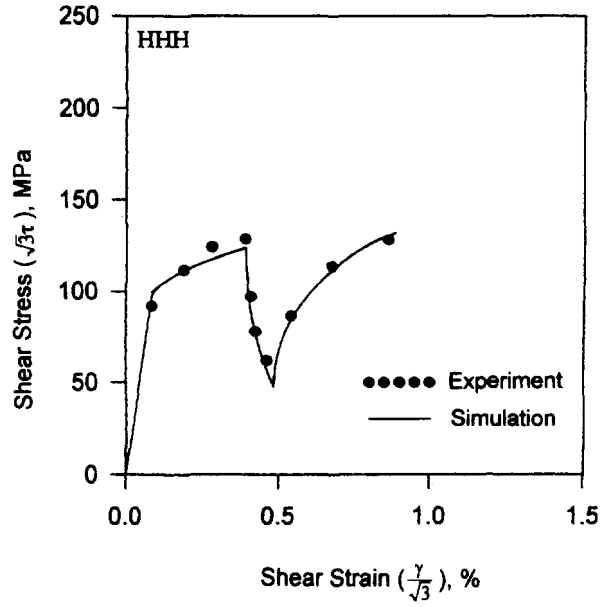

Fig. 14. Experimental and theoretical results of the shear stress–strain curve for 304 stainless steel under HHH loading condition.

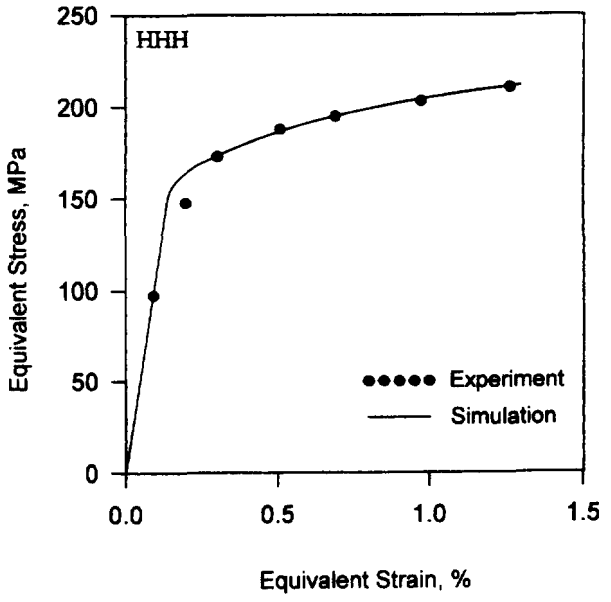

Fig. 15. Experimental and theoretical results of the equivalent stress–strain curve for 304 stainless steel under HHH loading condition.

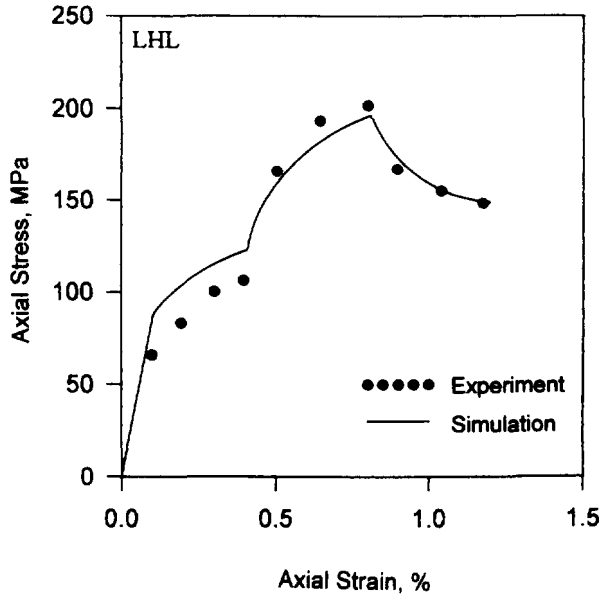

Fig. 16. Experimental and theoretical results of the axial stress–strain curve for 304 stainless steel under LHL loading condition.

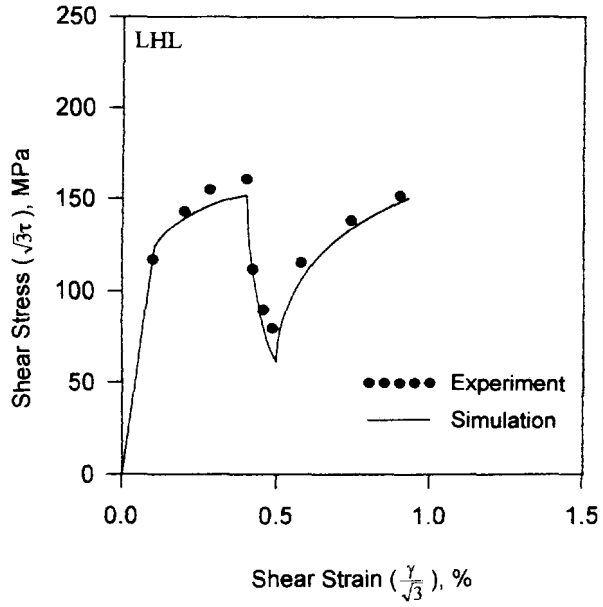

Fig. 17. Experimental and theoretical results of the shear stress–strain curve for 304 stainless steel under LHL loading condition.

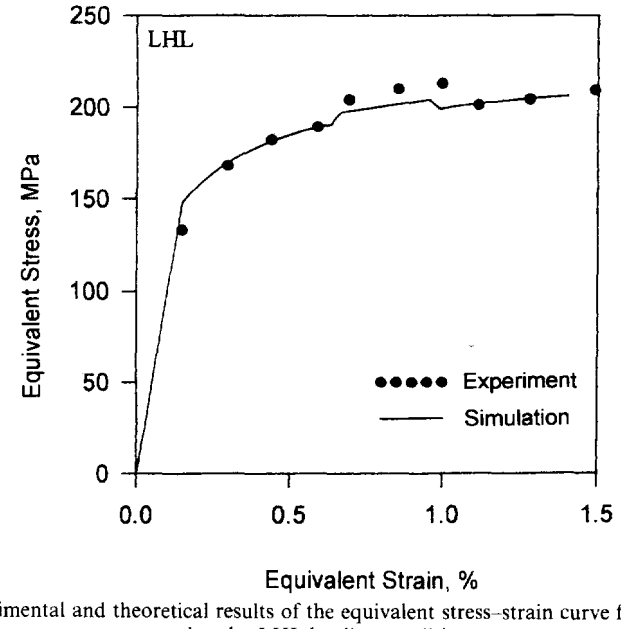

Fig. 18. Experimental and theoretical results of the equivalent stress–strain curve for 304 stainless steel under LHL loading condition.

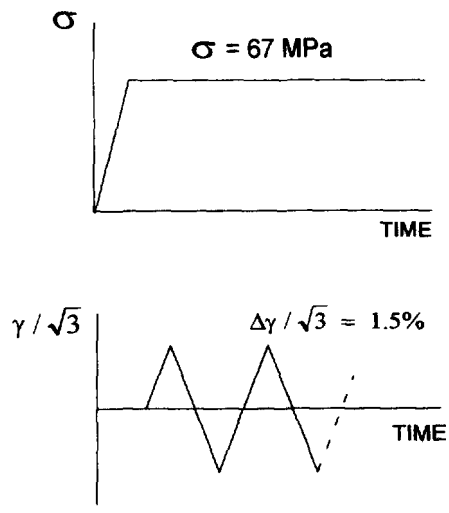

	Shear Strain-Rate
H	0.1 %/sec
L	0.002 %/sec

Fig. 19. Strain path of cyclic torsional straining with a constant axial stress for 304 stainless steel tested by Inoue *et al.* (1985).

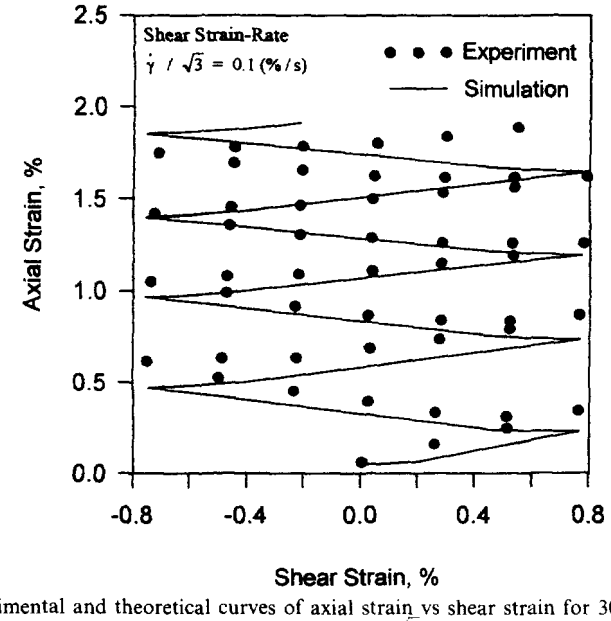

Fig. 20. Experimental and theoretical curves of axial strain vs shear strain for 304 stainless steel under the loading condition of $\dot{\gamma}/\sqrt{3} = 0.1\%\ s^{-1}$.

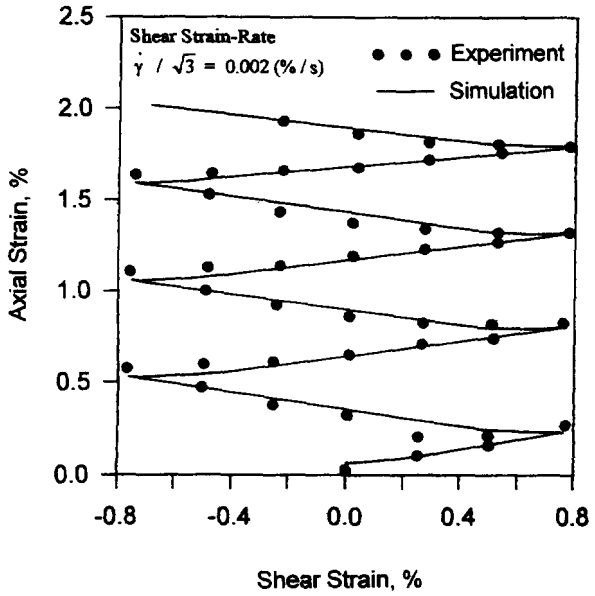

Fig. 21. Experimental and theoretical curves of axial strain vs shear strain for 304 stainless steel under the loading condition of $\dot{\gamma}/\sqrt{3} = 0.002\%\ s^{-1}$.

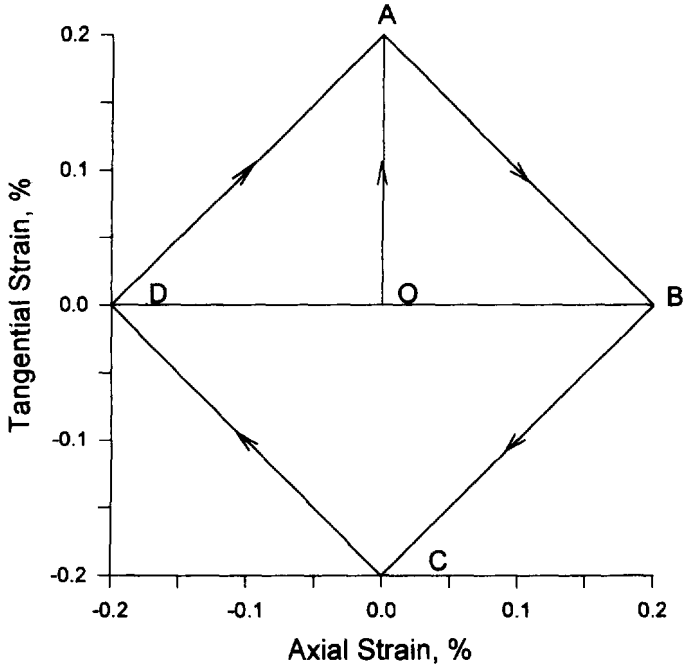

Fig. 22. The strain-path of the biaxial cyclic loading for 304 stainless steel tested by Ellyin *et al.* (1991).

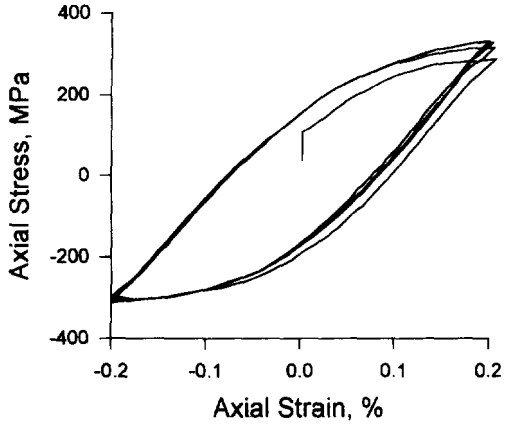

(a) Experiment

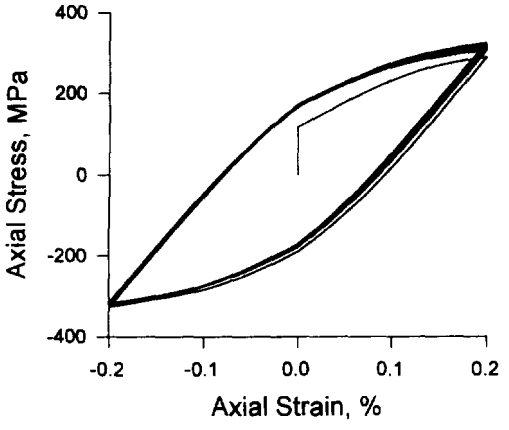

(b) Simulation

Fig. 23. Experimental and theoretical curves of the axial stress–strain response for 304 stainless steel at a strain-rate of $4 \times 10^{-3}\ s^{-1}$.

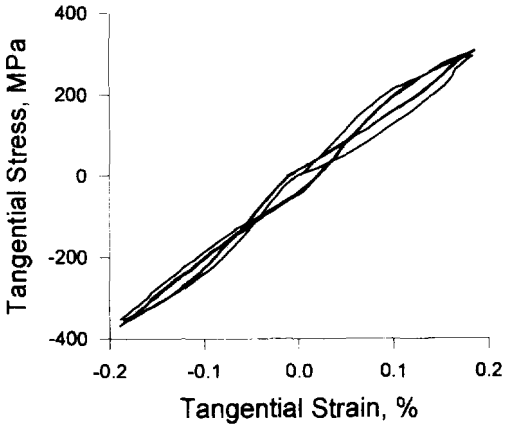

(a) Experiment

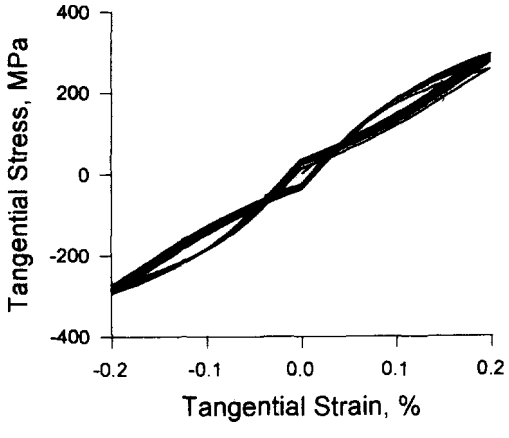

(b) Simulation

Fig. 24. Experimental and theoretical curves of the tangential stress–strain response for 304 stainless steel at a strain-rate of $4 \times 10^{-3}\ s^{-1}$.

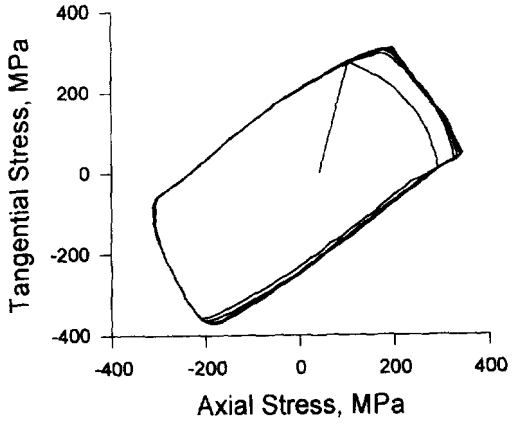

(a) Experiment

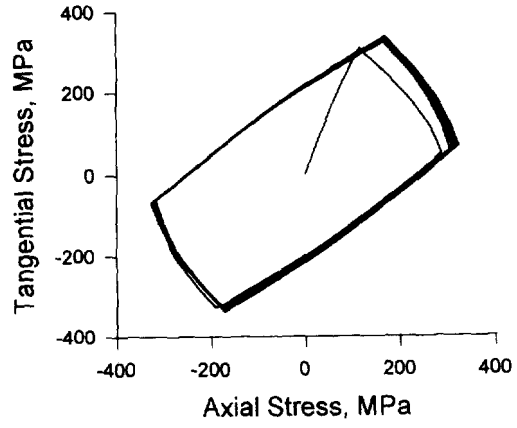

(b) Simulation

Fig. 25. Experimental and theoretical curves of the tangential stress and axial stress response for 304 stainless steel at a strain-rate of $4 \times 10^{-3}\ s^{-1}$.

REFERENCES

Bazant, Z. P. and Bhat, P. D. (1976). Endochronic theory of inelasticity and failure for concrete. *Journal of Engineering Mechanics ASME* **102,** EM4, 701–722.

Ellyin, F., Xia, Z. and Sasaki, K. (1991). Rate-dependent plastic deformation-experiments and constitutive modelling. *Proceedings of PLASTICITY '91, The 3rd International Symposium on Plasticity and Its Current Applications*, Grenoble, France, pp. 439–442.

Fan, J. (1983). A comprehensive numerical study and experimental verification of endochronic plasticity. Ph.D. Dissertation, Department of Aerospace Engineering and Applied Mechanics, University of Cincinnati.

Fan, J. and Peng, X. (1991). A physically based constitutive description for nonproportional cyclic plasticity. *Journal of Engineering Materials Technology* **113,** 254–262.

Im, S. and Atluri, S. N. (1987). A study of two finite strain plasticity models: an internal time theory using Mandel's director concept and a general isotropic/kinematic-hardening theory. *International Journal of Plasticity* **3,** 163–191.

Imai, G. and Xie, C. (1990). An endochronic constitutive law for static shear behavior of overconsolidated clays. *Soils and Foundations, Japanese Society Soil Mechanics and Foundation Engineering* **30**(1), 65–75.

Inoue, T., Imatani, S. and Sahashi, T. (1985) On the plasticity creep interaction behavior of SUS 304 steel under combined stress state of tension and torsion. *The 28th Japan Congress on Material Research*, pp. 15–22.

Krempl, E. (1979). An experimental study of room-temperature rate-sensitivity, creep and relaxation of AISI 304 stainless steel. *Journal of the Mechanics and Physics of Solids* **27,** 363–375.

Lamba, H. S. and Sidebottom, O. M. (1978) Cyclic plasticity for non-proportional paths: part 1—cyclic hardening, erasure of memory and subsequent strain hardening experiments. *Journal of Engineering Materials Technology* **100,** 96–103.

Lin, H. C. and Wu, H. C. (1976). Strain-rate effect in the endochronic theory of viscoplasticity. *Journal of Applied Mechanics* **98,** 92–96.

Lin, H. C. and Wu, H. C. (1983). On the rate-dependent endochronic theory of viscoplasticity and its application to plastic-wave propagation. *International Journal of Solids and Structures* **19**(7), 587–599.

Mathison, S. R., Pindera, M. J. and Herakovich, C. T. (1991). Nonlinear response of resin matrix laminates using endochronic theory. *Journal of Engineering Materials Technology* **113,** 449–455.

Murakami, H. and Read, H. E. (1987). Endochronic plasticity: some basic properties of plastic flow and failure. *International Journal of Solids and Structures* **23**(1), 133–151.

Murakami, H. and Read, H. E. (1989). A second-order numerical scheme for integrating the endochronic plasticity equations. *Computers and Structures* **31,** 663–672.

Valanis, K. C. (1971). A theory of viscoplasticity without a yield surface, part I—general theory; part II—application to mechanical behavior of metals. *Archives Mechanics* **25,** 517–551.

Valanis, K. C. (1977). Proper tensorial formulation of the internal variable theory—the endochronic time spectrum. *Archives Mechanics* **29,** 173–185.

Valanis, K. C. (1978). Endochronic theory of plastic fluids—metals under large deformation. *Applications of Numerical Methods to Forming Processes, ADM* 28 (ed. H. Armen), The American Society of Mechanical Engineers, pp. 47–58.

Valanis, K. C. (1979). Endochronic theory with proper loop closure properties. *System Science and Software Report SSS-R*-80-4182.

Valanis, K. C. (1980). Fundamental consequence of a new intrinsic time measure-plasticity as a limit of the endochronic theory. *Archives Mechanics* **32,** 171–191.

Valanis, K. C. (1984). Continuum foundations of plasticity. *ASME Journal of Engineering Materials Technology* **106,** 367–375.

Valanis, K. C. and Fan, J. (1983). Endochronic analysis of cyclic elastoplastic strain fields in a notched plate. *Journal of Applied Mechanics* **50,** 789–794.

Valanis, K. C. and Lee, C. F. (1984). Endochronic theory of cyclic plasticity with applications. *Journal of Applied Mechanics* **51,** 367–374.

Valanis, K. C. and Read, H. E. (1986). An endochronic plasticity theory for concrete. *Mechanics of Materials* **5,** 177–295.

Watanabe, O. and Atluri, S. N. (1985). A new endochronic approach to computational elasto-plasticity: an example of cyclically loaded cracked plate. *Journal of Applied Mechanics* **52,** 857–864.

Watanabe, O. and Atluri, S. N. (1986). Constitutive modeling of cyclic plasticity and creep, using an internal time concept. *International Journal of Plasticity* **2**(2), 107–134.

Wu, H. C. and Yip, M. C. (1980). Strain-rate and strain-rate history effects on the dynamic behavior of metallic materials. *International Journal of Solids and Structures* **16,** 515–536.

Wu, H. C. and Yip, M. C. (1981). Endochronic description of cyclic hardening behavior for metallic material. *Journal of Engineering Materials Technology* **103,** 212–217.

Wu, H. C. and Yang, R. J. (1983). Application of the improved endochronic theory of plasticity to loading with multi-axial strain path. *International Journal of Nonlinear Mechanics* **18,** 395–408.

Wu, H. C. and Wang, T. P. (1983). Endochronic modeling for shear hysteresis of sand. *Journal of Geotechnical Engineering* **109**(4) 970–981.

Wu, H. C. and Sheu, J. C. (1983). Endochronic description of sand response to static loading. *Journal of Engineering Mechanics* **109**(12), 1539–1550.

Wu, H. C. and Aboutorabi, M. R. (1988). Endochronic model of sand with circular stress path. *Journal of Geotechnical Engineering* **114**(1), 95–105.

Wu, H. C. and Yeh, W. C. (1988). Some consideration in the endochronic description of anisotropic hardening. *Acta Mechanica* **69,** 59–65.

Wu, H. C., Yang, C. C. and Chu, S. C. (1985). Further applications of endochronic constitutive equation to loading with non-proportional axial-torsional strain-path. *International Journal of Nonlinear Mechanics* **20,** 41–52.

Wu, H. C., Wang, Z. K. and Aboutorabi, M. R. (1985). Endochronic modeling of sand in true triaxial test. *Journal of Engineering Mechanics* **111**(10), 1257–1268.

Wu, H. C., Wang, T. P., Pan, W. F. and Xu, Z. Y. (1990). Cyclic stress–strain response of porous aluminum. *International Journal of Plasticity* **6,** 207–230.

Wu, H. C., Lu, J. K. and Pan, W. F. (1995). Endochronic equations for finite plastic deformation and application to metal tube under torsion. *International Journal of Solids and Structures* **32**(8/9), 1079–1097.

Yoshida, F. (1989). Viscoplastic behavior of SUS304 stainless steel under cyclic loading at room temperature and its phenomenological description. *Proceedings of PLASTICITY '89, the 2nd International Symposium on Plasticity and its Current Applications* (eds Khan, A. S. and Tokuda, M.), Mei, Japan, pp. 277–280.